

Comparative study of photothermal ablation of cancer cells with nuclear-targeted or cytoplasm-targeted gold nanospheres: continuous wave or pulsed lasers

Xiaohua Huang

Georgia Institute of Technology
School of Chemistry and Biochemistry
Laser Dynamics Laboratory
901 Atlantic Drive
Atlanta, Georgia 30332
and

The University of Memphis
Department of Chemistry
411 Smith Chemistry Building
Memphis, Tennessee 38152

Bin Kang

Wei Qian

Megan A. Mackey

Georgia Institute of Technology
School of Chemistry and Biochemistry
Laser Dynamics Laboratory
901 Atlantic Drive
Atlanta, Georgia 30332

Po C. Chen

Adegboyega K. Oyelere

Georgia Institute of Technology
Parker H. Petit Institute for Bioengineering and Biosciences
and
Georgia Institute of Technology
School of Chemistry and Biochemistry
901 Atlantic Drive
Atlanta, Georgia 30332

Ivan H. El-Sayed

University of California at San Francisco
Comprehensive Cancer Center
Otolaryngology-Head and Neck Surgery
521 Parnassus Avenue
San Francisco, California 94143

Mostafa A. El-Sayed

Georgia Institute of Technology
School of Chemistry and Biochemistry
Laser Dynamics Laboratory
901 Atlantic Drive
Atlanta, Georgia 30332

1 Introduction

Photothermal therapy (PTT), one of the major modalities for the treatment of cancer, has experienced a tremendous revolution from traditional laser therapy¹ to nanotechnology-driven photothermal ablation.²⁻⁴ Recently, gold-based plasmonic nanoparticles have shown great promise for use in photother-

Abstract. We conduct a comparative study on the efficiency and cell death pathways of continuous wave (cw) and nanosecond pulsed laser photothermal cancer therapy using gold nanospheres delivered to either the cytoplasm or nucleus of cancer cells. Cytoplasm localization is achieved using arginine-glycine-aspartate peptide modified gold nanospheres, which target integrin receptors on the cell surface and are subsequently internalized by the cells. Nuclear delivery is achieved by conjugating the gold nanospheres with nuclear localization sequence peptides originating from the simian virus. Photothermal experiments show that cell death can be induced with a single pulse of a nanosecond laser more efficiently than with a cw laser. When the cw laser is applied, gold nanospheres localized in the cytoplasm are more effective in inducing cell destruction than gold nanospheres localized at the nucleus. The opposite effect is observed when the nanosecond pulsed laser is used, suggesting that plasmonic field enhancement of the nonlinear absorption processes occurs at high localization of gold nanospheres at the nucleus. Cell death pathways are further investigated via a standard apoptosis kit to show that the cell death mechanisms depend on the type of laser used. While the cw laser induces cell death via apoptosis, the nanosecond pulsed laser leads to cell necrosis. These studies add mechanistic insight to gold nanoparticle-based photothermal therapy of cancer. © 2010 Society of Photo-Optical Instrumentation Engineers. [DOI: 10.1117/1.3486538]

Keywords: gold nanospheres; photothermal therapy; cancer; laser; apoptosis; necrosis.

Paper 09437RR received Sep. 29, 2009; revised manuscript received Jul. 2, 2010; accepted for publication Jul. 21, 2010; published online Oct. 29, 2010.

mal cancer therapy.⁵ The basic rationale is that gold nanospheres (Au NPs) absorb light orders of magnitude stronger than conventional organic dye molecules,⁶ due to their unique surface plasmon resonance^{7,8} (coherent collective oscillation of free electrons of the metal in resonance with the incident light). The strongly absorbed light is converted into heat quickly (on a picosecond time scale) and efficiently (nearly 100% of the absorbed light is converted to heat) by nonradi-

Address all correspondence to: Mostafa A. El-Sayed, 901 Atlantic Drive, Atlanta, Georgia 30332. Tel: 404-894-0292; Fax: 404-894-0294. Email: melsayed@gatech.edu

ative processes^{7–10} (i.e., electron-electron and electron-phonon interactions). Thus, under electromagnetic irradiation, the nanoparticles generate intense localized heat capable of destroying surrounding targeted cells. These thermal effects require minimal radiation exposure. Current gold analogs under study include spherical Au NPs (Refs. 11–18), gold nanoshells,^{2,19–23} gold nanorods,^{4,24–28} and gold nanocages.^{29–33}

To achieve cell- and site-specific delivery for the desired treatment, the nanoparticles must be functionalized with cargoes such as peptides, antibodies, and small molecule ligands for targeting. Arginine-glycine-aspartate (RGD)-peptide-conjugated nanoparticles have been shown to specifically bind to alpha v beta 3 integrin that are overexpressed on some types of cancer cells and tumor vasculature.^{34,35} On binding to these receptors, subsequent internalization via receptor-mediated endocytosis leads to intracellular accumulation of the nanoparticles in the cytoplasm. Nuclear targeting of nanoparticles can be particularly challenging, in that there are multiple barriers that exist from the cytoplasmic membrane to the nuclear envelope. To achieve sufficient nuclear targeting, assistance from nuclear translocation peptides, conjugated to the nanoparticles, is required; the nuclear localization signal (NLS) from the simian virus (SV) 40 large T antigen,^{36,37} adenovirus,^{38,39} and HIV Tat peptide.⁴⁰

Photothermally induced cell death can occur via apoptosis or necrosis, depending on the laser dosage, type, and irradiation time. It also depends on the subcellular location of the nanoparticles.^{16,26} Cell death mechanisms on photothermal treatment have been explored to some degree. For example, the studies of Ton et al.²⁶ showed that apoptosis is initiated by the disruption of the cytoplasmic membrane. Subsequent influx of calcium ions induces membrane blebbing and damage of actin filaments. In the work by Pustovalov et al.,¹⁶ laser pulses could induce cell damage by a series of photothermal and accompanied phenomena: denaturation and breakdown of proteins, cell cavitation, cellular structure rupturing, evaporation of cellular liquid and bubble formation by shock waves due to particle thermal expansion, and optical breakdown or plasma generation of Au NPs.

In this paper, we conduct a comparative study of the photothermal damage of cancer cells using continuous wave (cw) or nanosecond-pulsed lasers with Au NPs located at the nucleus or in the cytoplasm of the cell. Au NPs are conjugated with NLS (GGGPKKKRKVGG) peptides originating from the SV 40 large T antigen for nuclear localization and linear RGD peptides (RGDRGDRGDRGDPGC) for cytoplasm localization. The energy threshold and cell death pathways are determined and described according to the types of lasers and the location of Au NPs within the cell.

2 Materials and Methods

2.1 Synthesis of Au NPs and Peptide Conjugation

Citrate-capped Au NPs, 30 nm in diameter, were synthesized according to the citrate reduction method.^{41,42} Briefly, 50 mL of a 0.01% (by weight) auric acid (HAuCl₄, Sigma-Aldrich) aqueous solution was heated to boiling while stirring in a 100-mL beaker. A 350- μ L volume of a 1% (by weight) trisodium citrate (Sigma-Aldrich) aqueous solution was quickly added and the solution changed color within several minutes

(yellow to black to red), indicating nanoparticle formation. The surface plasmon absorption spectrum of the nanoparticle solution was measured with a UV-Vis spectrometer (Ocean Optics). Nanoparticle size was determined by transmission electron microscopy (TEM) and dynamic light scattering (DLS) using the Zeta Potential Instrument ZetaSizer Nano ZS90. Prior to peptide conjugation, Au NPs were modified with poly(ethylene) glycol (PEG). This was done by mixing 0.8 nM citrate-capped Au NPs (concentration calculated using $\epsilon_{\text{abs}} = 3.0 \times 10^9 \text{ M}^{-1} \text{ cm}^{-1}$ as determined by Hurst et al.⁴³) with 2 μ M mPEG-SH 5000 (methoxy-PEG, MW 5000, Laysan Bio Inc.) for 2 h at room temperature. The PEGylated nanoparticles were centrifuged at 14,000 rpm for 20 min and redispersed in phosphate-buffered saline (PBS) to a final optical density of 2.0. Citrate-capped Au NPs exhibit a zeta potential around -35 mV. After PEGylation, the zeta potential of Au NPs decreases to -8 mV. Having a nearly neutral charge, the PEG serves to prevent nonspecific adsorption of proteins to the nanoparticles in a physiological environment. To maximize the number of peptides that will bind to the nanoparticles, the amount of PEG molecules on the nanoparticles should be minimized. Here, the loading ratio of PEG molecules to Au NPs is ~ 2500 PEG molecules per nanoparticle, which is much lower than the number of PEG molecules (~ 8000) on a gold surface for a densely packed monolayer of 30 nm Au NPs (as estimated by an SPDP assay). With minimal PEG molecules on the Au NP surface, the thiolated peptides are able to bind to unoccupied sites on the Au NPs via Au-S bonds.

To facilitate binding to Au NPs, NLS peptides were functionalized with thiol linkers, as described in previous work,³⁶ and (RGD)₄ was modified with a cysteine residue. The thiol-modified NLS or RGD was mixed with PEGylated Au NPs to a final peptide concentration of 50 μ M and allowed to react overnight. The peptide-conjugated Au NPs were purified by centrifugation at 14,000 rpm for 20 min and redispersed in PBS buffer.

2.2 Cell Culture and Cellular Incubation with Au NPs

Human oral squamous cell carcinoma (HSC-3) cells were cultured in Dulbecco's modification of Eagle's medium (DMEM, Cellgro) with 10% fetal bovine serum (FBS, Gem Cell) at 37 °C under 5% CO₂. The cells were cleaved from the culture dish by trypsin and replated onto 18-mm glass coverslips in a 12-well tissue culture plate to grow for 2 days. The coverslips were coated with collagen type I (Roche), in advance, for optimum cell growth. Peptide-conjugated Au NPs [optical density (OD)=2 at 526 nm] were then added to each well at a volume of 200 μ L and cells were returned to 37 °C under 5% CO₂ for 24 h. The final concentration of Au NPs in cell culture medium was 0.2 nM, as previously reported for PTT using Au NPs *in vitro*.¹² After incubation, the cells on the glass coverslips were washed with PBS to remove excess Au NPs before further treatments.

2.3 Photothermal Treatment

In this study, two types of lasers were used for photothermal therapy: a cw argon ion laser with a 514-nm wavelength and a Q-switched Nd:YAG nanosecond-pulsed laser with a

532-nm wavelength. Note that the absorption peak of gold nanospheres is at 526 nm, the OD at 514 nm is about 94.5% of the OD at 532 nm, thus, the difference in laser wavelength here might not affect the difference in the energy threshold between the cw and pulsed lasers. The single pulse of the nanosecond laser was achieved by the *Q*-switched control, and the pulse width was about 6 to 7 ns. For the irradiation experiment, both the cw and pulsed lasers were focused to 1 mm in diameter at the sample position. Multiple regions of the cell monolayer were exposed to the cw laser beam at different energy densities for 5 min each and to a single nanosecond laser pulse with different energy. All experiments are repeated at least 3 times for energy threshold determinations to confirm reproducibility. Immediately following laser treatment, the cells are stained with 0.4% trypan blue (Sigma) for 10 min. Dead cells were stained blue due to the accumulation of the dye, while live cells remained unstained. For easy comparison, the total energy input is used to compare the energy threshold between the cw and pulsed lasers.

2.4 Fluorescence Staining and Imaging

To investigate the pathways of cell death on laser treatment, a double-stain (molecular probe) was used to distinguish between cell necrosis and apoptosis. The apoptotic cells were stained with annexin V-Alexa Fluor 488 (AV), while necrotic cells were stained with propidium iodide (PI). A 10 μL volume of AV (100 $\mu\text{g}/\text{mL}$) and a 5 μL volume of PI (100 $\mu\text{g}/\text{mL}$) were added to cells in 100 μL of annexin-binding buffer and incubated at room temperature for 15 min. After staining, cells were washed with PBS and fixed with a 4% paraformaldehyde solution. Fluorescence images were taken using an Olympus IX 70 microscope equipped with an argon ion laser. The excitation wavelength was 488 nm and the laser power was 100 mW.

3 Results and Discussion

3.1 Selective Intracellular Delivery of Peptide-Conjugated Au NPs

Au NPs were modified with NLS and linear (RGD)₄ peptides for cell nuclei and cytoplasm targeting, respectively. The conjugation was done by binding thiolated NLS and cysteine-modified RGD peptides to Au NPs that were stabilized with a minimal amount of thiolated methyl-poly (ethylene) glycol 5000 (mPEG-SH 5000) in advance. The pre-PEGylation serves two functions: (1) to decrease the surface charge of the citrate-capped Au NPs so as to avoid particle aggregation when the nanoparticles are exposed to oppositely charged peptides and (2) to minimize particle-cell nonspecific interactions, as citrate-capped Au NPs have shown to be internalized by both normal and cancer cells with high efficiency.⁴⁴

Figure 1 shows dark-field light scattering images of HSC-3 cells after a 24-h incubation (37 °C) with NLS-modified Au NPs (NLS/Au NPs) [Fig. 1(a)] and RGD-modified Au NPs (RGD/Au NPs) [Fig. 1(b)]. While NLS/Au NPs were dominantly localized at the cell nucleus, the RGD/Au NPs were distributed throughout the cytoplasm. This phenomenon was seen in over 80% of cells for several trials of this study. These observations can be attributed to the ability of the virus mimetic NLS to deliver nanocarriers to the cell nucleus via its

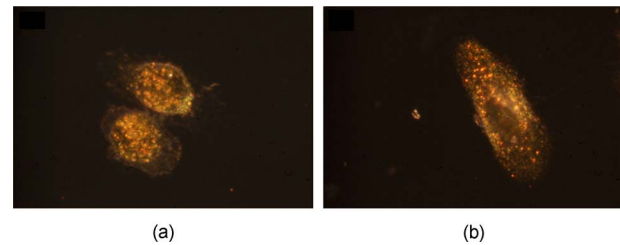


Fig. 1 Dark-field light scattering images: (a) NLS/Au NPs localize at the nucleus of HSC-3 cells and (b) RGD/Au NPs distribute throughout the cytoplasm of HSC-3 cells. Cells were incubated for 24 h at 37 °C with nanoparticles in cell culture medium. Scale bar: 10 μm .

binding to importin proteins on the nuclear envelope⁴⁵ and the ability of RGD to enable intracellular incorporation of particles via receptor-mediated endocytosis on binding to integrin receptors on the cell membrane of cancer cells.⁴⁶

3.2 Energy Threshold of Photothermal Therapy

3.2.1 Au NPs localized at the nucleus

For *in vivo* and clinical applications, it is favorable to use a minimal amount of energy in PTT so as not to damage surrounding healthy tissue. In this study, we determined the energy threshold required for cell destruction, utilizing trypan blue staining for detection of dead cells. Figure 2 displays bright-field images of cells (incubated with NLS/Au NPs) after single-pulse nanosecond laser treatment at different energies. It is apparent here that a single pulse (pulse duration: 6 to 7 ns) with an energy threshold of 0.3 to 0.45 mJ can induce cell death (Fig. 2, top right). In the control experiment (data not shown), in which the cells were not treated with Au NPs, a single pulse with a minimum energy of 3.3 to 3.9 mJ was required to induce cell death. This is approximately 10 times higher than that required for NLS/Au-NP-treated cells. Such improvement in the photothermal efficiency by treatment with NLS/Au NPs is undoubtedly due to the laser heating of Au NPs localized at the nucleus. The wavelength of the nanosecond laser (532 nm) overlaps with the surface plasmon absorption band of the Au NPs (absorption maximum around 526 nm). The surface plasmon absorption of the laser light by the Au NPs ensures efficient light energy conversion to ther-

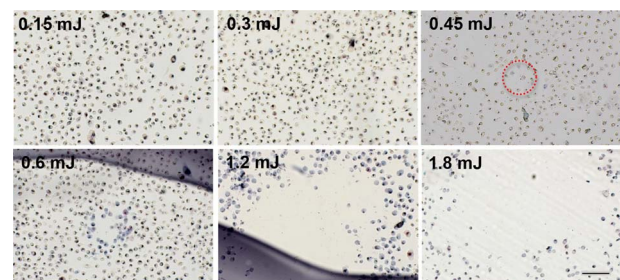


Fig. 2 Bright-field images of PTT of HSC-3 cells, in the presence of nuclear targeting Au NPs (NLS/Au NPs), by a single-pulse nanosecond laser at different energies. The energy threshold required to induce cell death is about 0.3 to 45 mJ per pulse (top right). Trypan blue staining is used for selective staining of dead cells (seen at energies of 0.45 mJ and higher). Scale bar: 100 μm . (Color online only.)

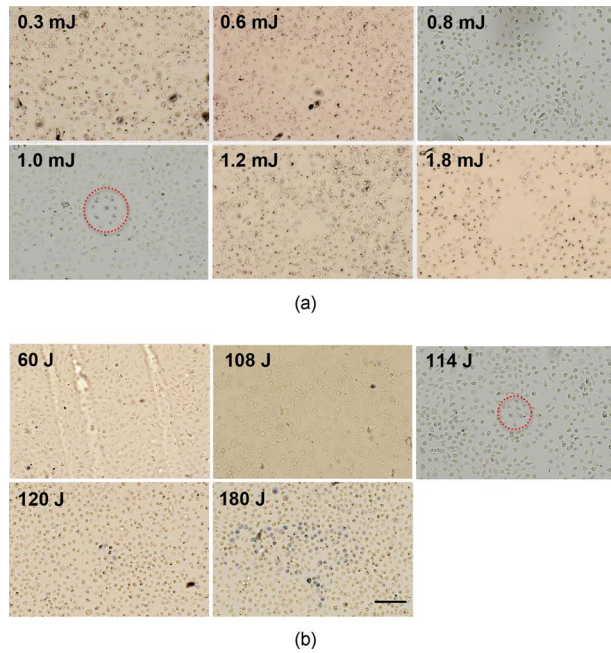


Fig. 3 Bright-field images of PTT of HSC-3 cells, in the presence of cytoplasm targeting Au NPs (RGD/Au NPs), by (a) a single-pulse nanosecond laser at different energies and (b) a cw laser at different energies. The energy threshold required to induce cell death with the nanosecond-pulsed laser is 0.8 to 1.0 mJ per pulse (a, bottom left). The energy threshold required to induce cell death with the cw laser is 108 to 114 J/mW (b, middle). Trypan blue staining is used for selective staining of dead cells. Scale bar: 150 μm . (Color online only.)

mal energy, which induces cell death via hyperthermia or cell ablation.

A cw argon ion laser with a wavelength of 514 nm and laser energy of 210 J was used to treat cells with Au NPs localized at the nucleus. We did not observe any dead cells under these conditions (images not shown). This laser energy is almost 4 times higher than the laser energy required to destroy cells with Au NPs localized on the cytoplasmic membrane¹² (60 J). Such a difference clearly shows that the location of Au NPs affects the photothermal efficiency to a great degree.

3.2.2 Au NPs located in the cytoplasm

Figure 3 displays bright-field images of cells (incubated with RGD/Au NPs) after treatment with pulsed nanosecond [Fig. 3(a)] and cw [Fig. 3(b)] lasers. In the case of the nanosecond-pulsed laser treatment, the energy threshold (minimum energy at which cell death occurs) was 0.8 to 1.0 mJ [Fig. 3(a), bottom left] with a single pulse (pulse duration: 6 to 7 ns), which is almost 3 times the energy threshold for cells with Au NPs localized at the nucleus. With this observation, it is apparent that the location of Au NPs, either at the nucleus or throughout the cytoplasm, determines the laser energy required to induce cell death. As shown in the dark-field light scattering images in Fig. 1, Au NPs are more localized in cells with NLS/Au NPs, but more dispersed in cells with RGD/Au NPs. Note that in these experiments, the same concentration of peptide conjugated Au NPs was used for the two cases and all other parameters were controlled. Therefore, the close pack-

ing (aggregation) of Au NPs at the nucleus must generate heat more efficiently, providing for a lower energy threshold. This might be due to two effects. First, an increased surface plasmon field is expected due to the aggregation of Au NPs at the nucleus. Second, the high laser intensity (due to short pulse width) enhances nonlinear absorption processes. These two effects make the energy absorbed during the pulse so high that it requires a lower threshold to destroy the cell.

In contrast to the nanosecond-pulsed laser, a cw laser requires a much lower energy to induce cell death when Au NPs are in the cytoplasm compared to Au NPs at the nucleus. As seen in Fig. 3, at 108 to 114 J [Fig. 3(b), middle], cell damage is achieved with Au NPs in the cytoplasm, whereas 210 J did not induce cell destruction with Au NPs localized at the nucleus (data not shown), as we described in the previous section. This contrast could be due to the difference in the amounts of effective energy delivered to the cell from the two different lasers. This depends on the laser power and plasmon field intensity, which depends on the degree of nanoparticle aggregation. These factors may also dictate the cell death mechanisms involved when using the different types of lasers.

In summary, the energy threshold for the pulsed nanosecond laser is about 500,000 times lower than that for the cw laser when Au NPs are localized at the nucleus, and about 100,000 times lower when Au NPs are dispersed throughout the cytoplasm. In general, when Au NPs are localized at the nucleus, a lower energy nanosecond laser pulse is required to induce cell death than when Au NPs are dispersed throughout the cytoplasm, but the opposite is true when the cw laser is used. Previous results¹² showed that when Au NPs are localized on the cell membrane, the intensity threshold required to induce cell death with the cw laser is 25 W/cm² (60 J), which is lower than that required when Au NPs are in the cytoplasm (108 to 114 J), as determined here. Tong et al. also reported similar results using folate-targeted gold nanorods.²⁶ Such a phenomenon could be due to the arrangement and the density of the nanoparticles on the cell membrane and the potential for aggregation of Au NPs, resulting in a stronger surface plasmon absorption of light and thus more efficient photothermal effects.

Photoacoustic effects could potentially be the cause of cell death for the nanosecond-pulsed laser treatments displayed here. On irradiation with a laser pulse, the compact Au NPs at the nucleus could produce highly localized heat, generating acoustic waves.¹⁶ This could cause mechanical damage to the cell via the formation of bubbles inside cells. Multiphoton processes could also take place, leading to the dissociation and ionization of nucleic acid bases, thereby destroying DNA or protein molecules.

3.3 Cell Death Pathways

3.3.1 Au NPs localized at the nucleus

Because laser-induced cell death was observed, as already discussed, it is important to investigate the mechanisms by which cell death occurs. To do so, a standard apoptosis kit was used. The kit contains a probe for cells that exhibit early apoptosis (AlexaFluor 488 AV) and a probe for cells that are necrotic (PI). Figure 4 shows bright-field images after trypan blue staining and fluorescence images after AV/PI staining of the cw [Fig. 4(a)] and nanosecond pulsed laser [Fig. 4(b)] treated

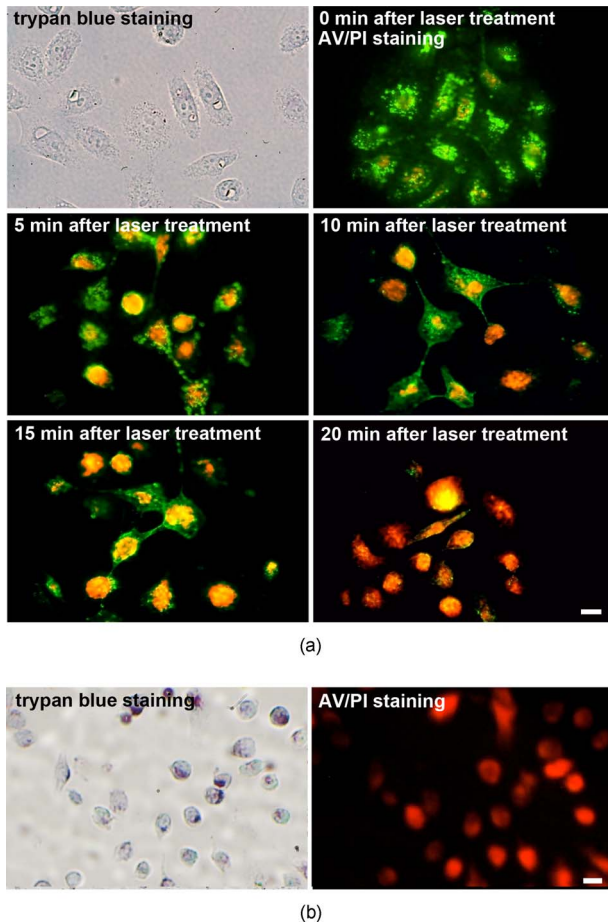


Fig. 4 Bright-field and fluorescence images of the investigation of cell death pathways that occur on laser treatment of cells incubated with nuclear localized Au NPs (NLS/Au NPs) using (a) the cw laser and (b) the nanosecond-pulsed laser. For the cw laser treatment (a), the total energy is 180 J. For nanosecond-pulsed laser treatment (b), an total energy of 0.6 mJ is used. Trypan blue staining is used for selective staining of dead cells detected in the bright-field images. AV/PI fluorescence staining is used for selective staining of apoptotic/necrotic cells in the fluorescence images. With cw laser treatment (a), the death of cells gradually progresses from early apoptosis, indicated by AV staining (top right), to necrosis, indicated by PI staining (bottom right). With nanosecond-pulsed laser treatment (b), the death of cells occurs via necrosis immediately after laser treatment, indicated by PI staining (right). Scale bar: 20 μm . (Color online only.)

cells with Au NPs localized at the nucleus. As stated in the previous section, cell death does not occur (no accumulation of trypan blue in cells) even at a cw laser energy of 180 J [Fig. 4(a), bright-field image], indicating that the cell membrane is intact during cw laser treatment. However, the cells in this case display AV/PI fluorescence when 180 J is used [Fig. 4(a)]. Immediately following cw laser treatment, the cells were stained green by AV, indicating an early stage of apoptosis. Cell membrane alterations can occur during the initial stages of apoptosis, namely the translocation of phosphatidylserine (PS) (normally located on the cytoplasmic side of the cell membrane) to the external surface of the cell. The Ca^{2+} -dependent phospholipid-binding protein, AV, has a high affinity for PS and can thus probe for early apoptosis. At later times following cw laser treatment, a time-dependent PI stain-

ing of the cells occurs. PI is a DNA-binding dye that is not cell membrane permeable and thus distinguishes necrotic cells from apoptotic cells. From the fluorescence images at different time points following laser treatment [Fig. 4(a), middle and bottom] the progression of cells from early apoptosis to necrosis is apparent as the fluorescence changes from green (AV), to yellow (AV and PI), and finally to red (PI). (Color online only.)

Apoptosis is not observed when a nanosecond-pulsed laser is used for the treatment of cells with Au NPs localized at the nucleus. At a pulsed laser energy of 0.1 to 0.3 mJ (below the threshold of 0.3 to 0.45 mJ), no apoptosis was observed. On increasing the pulsed laser energy to 0.6 mJ, only PI (red fluorescence) accumulation in cells is observed [Fig. 4(b), right], indicating that the higher energy nanosecond laser pulse induced cell death via necrosis. This immediate cell death is due to the strong and rapid heating of Au NPs by the nanosecond laser pulse, which could produce shock waves¹⁶ that damage the cells in a very short time. The absence of green fluorescence from AV staining, in this case, might be due to the nanosecond laser pulse inducing severe damage to the cell membrane, which would make the binding of AV to PS difficult.

3.3.2 Au NPs located in the cytoplasm

Figure 5 shows bright-field images after trypan blue staining and fluorescence images after AV/PI staining of the cw [Fig. 5(a)] and nanosecond-pulsed laser [Fig. 5(b)] treated cells with Au NPs dispersed throughout the cytoplasm. When the cw laser energy was at 60 J (below the threshold of 120 J), cells were not stained by trypan blue, even with a 10-min laser irradiation, indicating that the laser treatment did not cause cell membrane damage. The fluorescence images at different time points after the laser treatment showed the progression of cells from early- to late-stage apoptosis (not reaching complete necrosis). When the cw laser energy was higher, 120 J [Fig. 5(a), bottom], the dead cells are stained by both trypan blue and PI, indicating cell membrane damage and resulting in necrosis of the cells. The cell death mechanism's dependence on laser energy, as seen here, was also observed by other researchers²⁸ when folate-targeted gold nanorods were delivered to the cytoplasm of cancer cells.

Similar to the results obtained when Au NPs are localized at the nucleus, the nanosecond-pulsed laser immediately induced necrosis in cells with Au NPs distributed throughout the cytoplasm, as indicated by the accumulation of PI in the cells [Fig. 5(b), right]. It is apparent, with this observation, that the location of the Au NPs within the cell does not determine the mechanism of cell death on nanosecond-pulsed laser treatments. However, when the cw laser is used, higher energy induces necrosis and lower energy induces apoptosis when Au NPs are located in cytoplasm, while no necrosis is observed when Au NPs are localized at the nucleus. This is most likely due to there not being sufficient laser energy for a necrosis process to occur.

4 Conclusion

In summary, Au NPs can selectively target the nucleus or the cytoplasm of HSC-3 (cancer) cells using NLS and linear RGD peptides, respectively. Photothermal studies show that the

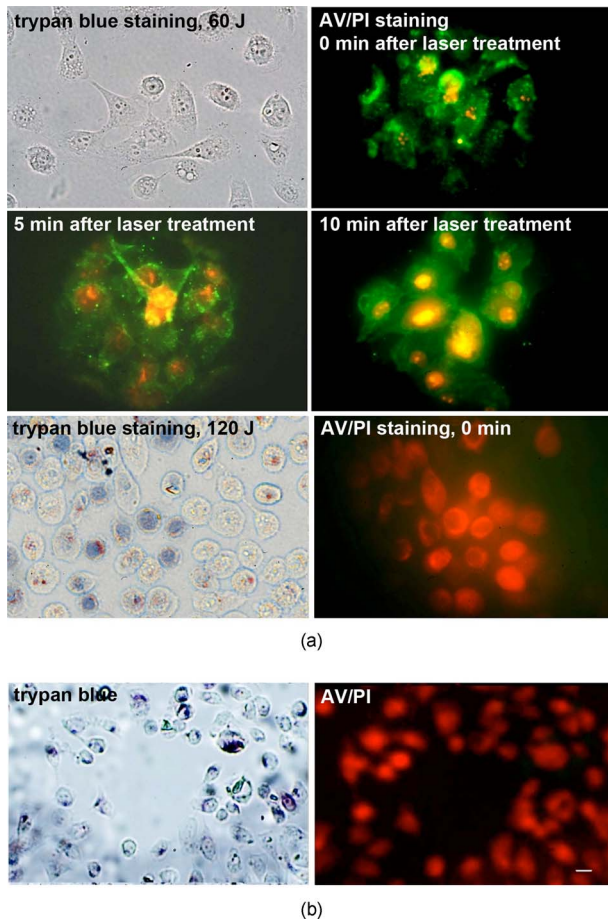


Fig. 5 Bright-field and fluorescence images of the investigation of cell death pathways on laser treatment of cells incubated with cytoplasm targeting Au NPs (RGD/Au NPs) using (a) the cw laser and (b) the nanosecond-pulsed laser. For cw laser treatment (a), a total energy of 60 J (top and middle) and 120 J (bottom) were used. For nanosecond-pulsed laser treatment (b), an energy of 1.2 mJ was used. Trypan blue staining was used for selective staining of dead cells detected in the bright-field images. AV/PI fluorescence staining was used for selective staining of apoptotic/necrotic cells in the fluorescence images. With cw laser treatment at 60 J (a, top and middle), the death of cells gradually progressed from early apoptosis, indicated by AV staining (top right), to late apoptosis, indicated by some PI staining (middle right). With cw laser treatment at 120 J (a, bottom), the death of cells occurred via necrosis immediately after laser treatment, indicated by PI staining (right). With nanosecond pulsed laser treatment (b), the death of cells occurred via necrosis immediately after laser treatment, indicated by PI staining (right). Scale bar: 20 μm . (Color online only.)

nanosecond-pulsed laser is more effective than the cw laser for purposes of inducing cell destruction, independent of the intracellular location of the Au NPs. Photothermal experiments also show that when treating cells with the cw laser, Au NPs are more successful at destroying cells when distributed in the cytoplasm than when localized at the nucleus, while the opposite is true with nanosecond-pulsed laser treatments. Fluorescence staining results indicate that when cells are treated with a cw laser, cell death is attributed to apoptosis with Au NPs localized at the nucleus and apoptosis or necrosis, depending on the laser intensity, with Au NPs in the cytoplasm. The nanosecond-pulsed laser treatments induce necrosis only, despite the location of the nanoparticles.

Acknowledgments

X. Huang would like to thank the distinguished CCNE post-doctoral fellowship at Emory-Georgia Tech Cancer Center for Nanotechnology Excellence, B. Kang thanks the support of China Scholarship Council (No. 2008683010) and Doctor Innovation Funds of NUAA (BCXJ08-09, China). I. H. El-Sayed thanks the Hearing Research Institute for financial support and M. A. El-Sayed thanks the honor of Julius Brown Chair at Georgia Tech.

References

1. R. A. Sultan, "Tumor ablation by laser in general surgery," *Lasers Med. Sci.* **5**(2), 185–193 (1990).
2. L. R. Hirsch, R. J. Stafford, J. A. Bankson, S. R. Sershen, R. E. Price, J. D. Hazle, N. J. Halas, and J. L. West, "Nanoshell-mediated near infrared thermal therapy of tumors under magnetic resonance guidance," *Proc. Natl. Acad. Sci. U.S.A.* **100**(23), 13549–13554 (2003).
3. N. W. S. Kam, M. O'Connell, J. A. Wisdom, and H. Dai, "Carbon nanotubes as multifunctional biological transporters and near-infrared agents for selective cancer cell destruction," *Proc. Natl. Acad. Sci. U.S.A.* **102**(33), 11600–11605 (2005).
4. X. Huang, I. H. El-Sayed, W. Qian, and M. A. El-Sayed, "Cancer cell imaging and photothermal therapy in the near-infrared region by using gold nanorods," *J. Am. Chem. Soc.* **128**(6), 2115–2120 (2006).
5. X. Huang, P. K. Jain, I. H. El-Sayed, and M. A. El-Sayed, "Plasmonic photothermal therapy (PPTT) using gold nanospheres," *Lasers Med. Sci.* **23**(3), 217–228 (2008).
6. P. K. Jain, K. S. Lee, I. H. El-Sayed, and M. A. El-Sayed, "Calculated absorption and scattering properties of gold nanospheres of different size, shape, and composition: applications in biological imaging and biomedicine," *J. Phys. Chem. B* **110**(14), 7238–7248 (2006).
7. S. Link and M. A. El-Sayed, "Shape and size dependence of radiative, non-radiative and photothermal properties of gold nanocrystals," *Int. Rev. Phys. Chem.* **19**(3), 409–453 (2000).
8. S. Link and M. A. El-Sayed, "Optical properties and ultrafast dynamics of metallic nanocrystals," *Annu. Rev. Phys. Chem.* **54**, 331–366 (2003).
9. S. Link and M. A. El-Sayed, "Spectral properties and relaxation dynamics of surface plasmon electronic oscillations in gold and silver nanodots and nanorods," *J. Phys. Chem. B* **103**(40), 8410–8426 (1999).
10. M. A. El-Sayed, "Some interesting properties of metals confined in time and nanometer space of different shapes," *Acc. Chem. Res.* **34**(4), 257–264 (2001).
11. V. P. Zharov, E. N. Galitovskaya, C. Johnson, and T. Kelly, "Synergistic enhancement of selective nanophotothermal therapy with gold nanoclusters: potential for cancer therapy," *Lasers Surg. Med.* **37**(3), 219–226 (2005).
12. I. H. El-Sayed, X. Huang, and M. A. El-Sayed, "Selective laser photo-thermal therapy of epithelial carcinoma using anti-EGFR antibody conjugated gold nanospheres," *Cancer Lett.* **239**(1), 129–135 (2006).
13. B. Khlebtsov, V. Zharov, A. Melnikov, V. Tuchin, and N. Khlebtsov, "Optical amplification of photothermal therapy with gold nanospheres and nanoclusters," *Nanotechnology* **17**, 5167–5179 (2006).
14. D. Pissuwan, C. H. Cortie, S. M. Valenzuela, and M. B. Cortie, "Gold nanosphere-antibody conjugates for hyperthermal therapeutic applications," *Gold Bull.* **40**(2), 121–129 (2007).
15. X. H. Huang, W. Qian, I. H. El-Sayed, and M. A. El-Sayed, "The potential use of the enhanced nonlinear properties of gold nanospheres in photothermal cancer therapy," *Lasers Surg. Med.* **39**(9), 747–753 (2007).
16. V. K. Pustovalov, A. S. Smetannikov, and V. P. Zharov, "Photothermal and accompanied phenomena of selective nanophotothermal therapy with gold nanospheres and laser pulses," *Laser Phys. Lett.* **5**(11), 775–792 (2008).
17. E. Y. Hleb, J. H. Hafner, J. N. Myers, E. Y. Hanna, B. C. Rostro, S. A. Zhdanok, and D. O. Lapotko, "Elimination of solid tumor cells with photothermal bubbles generated around clusters of gold nanospheres," *Nanomedicine* **3**(5), 647–667 (2008).
18. X. Liu, M. C. Lloyd, I. V. Fedorenko, P. Bapat, T. Zhukov, and Q. Huo, "Enhanced imaging and accelerated photothermal therapy of A549

- human lung cancer cells by gold nanospheres," *Nanomedicine* **3**(5), 617–626 (2008).
19. D. P. O'Neal, L. R. Hirsch, N. J. Halas, J. D. Payne, and J. L. West, "Photothermal tumor ablation in mice using near infrared absorbing nanoshells," *Cancer Lett.* **209**(2), 171–176 (2004).
 20. A. M. Gobin, M. H. Lee, N. J. Halas, W. D. James, R. A. Drezek, and J. L. West, "Near-infrared resonant nanoshells for combined optical imaging and photothermal cancer therapy," *Nano Lett.* **7**(7), 1929–1934 (2007).
 21. P. Diagaradjane, A. Shetty, J. C. Wang, A. M. Elliott, J. Schwartz, S. Shentu, H. C. Park, A. Deorukhkar, R. J. Stafford, S. H. Cho, J. W. Tunnell, J. D. Hazle, and S. Krishnan, "Modulation of in vivo tumor radiation response via gold nanoshell-mediated vascular-focused hyperthermia: characterizing an integrated antihypoxic and localized vascular disrupting targeting strategy," *Nano Lett.* **8**(5), 1492–1500 (2008).
 22. S. Lal, S. E. Clare, and N. J. Halas, "Nanoshell-enabled photothermal cancer therapy: impending clinical impact," *Acc. Chem. Res.* **41**(12), 1842–1851 (2008).
 23. C. Loo, A. Lowery, N. J. Halas, J. L. West, and R. Drezek, "Immunotargeted nanoshells for integrated cancer imaging and therapy," *Nano Lett.* **5**(4), 709–711 (2005).
 24. H. Takahashi, T. Niidome, A. Nariai, Y. Niidome, and S. Yamada, "Gold nanorod-sensitized cell death: microscopic observation of single living cells irradiated by pulsed near-infrared laser light in the presence of gold nanorods," *Chem. Lett.* **35**(5), 500–501 (2006).
 25. T. B. Huff, L. Tong, Y. Zhao, M. N. Hansen, J. X. Cheng, and A. Wei, "Hyperthermic effects of gold nanorods on tumor cells," *Nanomedicine* **2**(1), 125–132 (2007).
 26. L. Tong, Y. Zhao, T. B. Huff, M. N. Hansen, A. Wei, and J. X. Cheng, "Gold nanorods mediate tumor cell death by compromising membrane integrity," *Adv. Mater.* **19**(20), 3136–3141 (2007).
 27. J. L. Li, D. Day, and M. Gu, "Ultra-low energy threshold for cancer photothermal therapy using transferrin-conjugated gold nanorods," *Adv. Mater.* **20**(20), 3866–3871 (2008).
 28. L. Tong and J. X. Cheng, "Gold nanorod-mediated photothermolysis induces apoptosis of macrophages via damage of mitochondria," *Nanomedicine* **4**(3), 265–276 (2009).
 29. J. Chen, D. Wang, J. Xi, L. Au, A. Siekkinen, A. Warsen, Z. Y. Li, H. Zhang, Y. Xia, and X. Li, "Immuno gold nanocages with tailored optical properties for targeted photothermal destruction of cancer cells," *Nano Lett.* **7**(5), 1318–1322 (2007).
 30. L. Au, D. Zheng, F. Zhou, Z. Y. Li, X. Li, and Y. A. Xia, "Quantitative study on the photothermal effect of immuno gold nanocages targeted to breast cancer cells," *ACS Nano* **2**(8), 1645–1652 (2008).
 31. M. P. Melancon, W. Lu, Z. Yang, R. Zhang, Z. Cheng, A. M. Elliot, J. Stafford, T. Olson, J. Z. Zhang, and C. Li, "In vitro and in vivo targeting of hollow gold nanoshells directed at epidermal growth factor receptor for photothermal ablation therapy," *Mol. Cancer Ther.* **7**(6), 1730–1739 (2008).
 32. Y. T. Lim, M. Y. Cho, B. S. Choi, Y. W. Noh, and B. H. Chung, "Diagnosis and therapy of macrophage cells using dextran-coated near-infrared responsive hollow-type gold nanospheres," *Nanotechnology* **19**(37), 375105 (2008).
 33. W. Lu, C. Xiong, G. Zhang, Q. Huang, R. Zhang, J. Z. Zhang, and C. Li, "Targeted photothermal ablation of murine melanomas with melanocyte-stimulating hormone analog conjugated hollow gold nanospheres," *Clin. Cancer Res.* **15**(3), 876–886 (2009).
 34. W. Cai, D. M. Shin, K. Chen, O. Gheysens, Q. Cao, S. X. Wang, S. S. Gambhir, and X. Chen, "Peptide-labeled near-infrared quantum dots for imaging tumor vasculature in living subjects," *Nano Lett.* **6**(4), 669–676 (2006).
 35. B. R. Smith, Z. Cheng, A. De, A. L. Koh, R. Sinclair, and S. S. Gambhir, "Real-time intravital imaging of RGD-quantum dot binding to luminal endothelium in mouse tumor neovasculature," *Nano Lett.* **8**(9), 2599–2606 (2008).
 36. A. K. Oyelere, B. Chen, X. Huang, I. H. El-Sayed, and M. A. El-Sayed, "Peptide conjugated gold nanorods for nuclear targeting," *Bioconjugate Chem.* **18**(5), 1490–1497 (2007).
 37. A. G. Tkachenko, H. Xie, Y. Liu, D. Coleman, J. Ryan, W. R. Glomm, M. K. Shipton, S. Franzen, and D. L. Feldheim, "Cellular trajectories of peptide-modified gold particle complexes: comparison of nuclear localization signals and peptide transduction domains," *Bioconjugate Chem.* **15**(3), 482–490 (2004).
 38. A. G. Tkachenko, H. Xie, D. Coleman, W. Glomm, J. Ryan, M. E. Anderson, S. Franzen, and D. L. Feldheim, "Multifunctional gold nanoparticle-peptide complexes for nuclear targeting," *J. Am. Chem. Soc.* **125**(16), 4700–4701 (2003).
 39. P. Nativo, I. A. Prior, and M. Brust, "Uptake and intracellular fate of surface-modified gold nanospheres," *ACS Nano* **2**(8), 1639–1644 (2008).
 40. J. M. de la Fuente and C. C. Berry, "Tat peptide as an efficient molecule to translocate gold nanospheres into the cell nucleus," *Bioconjugate Chem.* **16**(5), 1176–1180 (2005).
 41. J. Turkevich, P. C. Stevenson, and J. Hillier, "A study of the nucleation and growth processes in the synthesis of colloidal gold," *Discuss. Faraday Soc.* **11**, 55–75 (1951).
 42. G. Frens, "Controlled nucleation for the regulation of the particle size in monodisperse gold suspensions," *Nature Phys. Sci.* **241**, 20–22 (1973).
 43. S. J. Hurst, A. K. R. Lytton-Jean, and C. A. Mirkin, "Maximizing DNA loading on a range of gold nanoparticle sizes," *Anal. Chem.* **78**(24), 8313–8318 (2006).
 44. I. H. El-Sayed, X. Huang, and M. A. El-Sayed, "Surface plasmon resonance scattering and absorption of anti-EGFR antibody conjugated gold nanospheres in cancer diagnostics: applications in oral cancer," *Nano Lett.* **5**(5), 829–834 (2005).
 45. S. Nakiely and G. Dreyfuss, "Transport of proteins and RNAs in and out of the nucleus," *Cell* **99**, 677–690 (1999).
 46. H. J. Gao, W. D. Shi, and L. B. Freund, "Mechanics of receptor-mediated endocytosis," *Proc. Natl. Acad. Sci. U.S.A.* **102**, 9469–9474, (2005).